Supplementary Information for

Morphology-independent general-purpose optical surface tractor beam

Neng Wang,[1] Jack Ng,[2,*] Guo Ping Wang[1,3,*]

[1]*State Key Laboratory of Radio Frequency Heterogeneous Integration, Shenzhen University, Shenzhen 518060, China*

[2]*Department of Physics, Southern University of Science and Technology, Shenzhen 518055, China*

[3]*College of Electronics and Information Engineering, Shenzhen University, Shenzhen 518060, China*

Corresponding to: wuzh3@sustech.edu.cn, gpwang@szu.edu.cn

Supplementary Note 1： General expression of the longitudinal optical force

In the main text, we derived an expression for the longitudinal optical force acting on the particle. This force can be calculated by integrating the Minkowski stress tensor $\ddot{\mathbf{T}}^{\min}$ over a closed surface S that encloses the particle. Specifically, the force can be written as:

$$F_x = \oiint_S \hat{x} \cdot \ddot{\mathbf{T}}^{\min} \cdot \hat{n} dS, \tag{S1}$$

where S is an arbitrary closed surface and $\hat{n}$ is the outward normal unit vector of S. To simplify the calculations, we choose the closed surface S to be a spherical surface S_∞ with an infinite radius $R \to \infty$, as illustrated in Supplementary Fig. 1.

In our analysis, we consider the metamaterial to be infinite in the *x* and *y* directions, while it extends indefinitely in the negative *z* direction. The incident surface wave (SW) is launched from the left infinity ($x \to \infty$). For convenience, we assume the metamaterial to be isotropic, characterized by a relative permittivity ε and permeability μ.

In this system, we have three types of electromagnetic (EM) waves: the incident surface wave (SW), the scattered SWs propagating in all directions on the *xoy* plane, and the freely propagating waves (FPWs) that propagate in all solid angles both in air and inside the metamaterial. For the incident SW, the electric and magnetic fields can be expressed as:

$$\mathbf{E}^{(i)} = (e_{ix}, e_{iy}, e_{iz})^T e^{ik_p x}, \quad \mathbf{H}^{(i)} = (h_{ix}, h_{iy}, h_{iz})^T e^{ik_p x}, \tag{S2}$$

where k_p is the propagating wavenumber of the SW, $e_{ix,y,z}$ and $h_{ix,y,z}$ are functions that depend on *z* only and vanish at the infinities ($z \to \pm\infty$). The superscript (*i*) denotes that these fields are associated with the incident SW. By applying Maxwell's equations, we can obtain the electric and magnetic induction fields of the incident SW:

$$\mathbf{D}^{(i)} = \frac{i}{\omega}\nabla\times\mathbf{H}^{(i)} = \frac{i}{\omega}(-\partial_z h_{iy}, \partial_z h_{ix} - ik_p h_{iz}, ik_p h_{iy})^T e^{ik_p x},$$
$$\mathbf{B}^{(i)} = -\frac{i}{\omega}\nabla\times\mathbf{E}^{(i)} = -\frac{i}{\omega}(-\partial_z e_{iy}, \partial_z e_{ix} - ik_p e_{iz}, ik_p e_{iy})^T e^{ik_p x}. \quad \text{(S3)}$$

The scattered SWs are confined to the *xoy* plane, and in the far field limit ($R\to\infty$), it is convenient to express their EM fields in cylindrical coordinates as:

$$\mathbf{E}^{(s)}(\phi) = (e_\rho, e_\phi, e_z)^T e^{ik_p\rho}, \quad \mathbf{H}^{(s)}(\phi) = (h_\rho, h_\phi, h_z)^T e^{ik_p\rho}. \quad \text{(S4)}$$

Here, $e_{\rho,\phi,z}$ and $h_{\rho,\phi,z}$ are functions that depend on the coordinates ρ,ϕ,z, and vanish in the limit $z\to\pm\infty$. These functions characterize the field amplitudes of the scattered SW. The superscript (*s*) denotes that these fields are associated with the scattered SW.

In the far field region ($\rho\to\infty$), the radiation boundary condition and energy conservation dictate that the functions $e_{\rho,\phi,z}$ and $h_{\rho,\phi,z}$ scale as $\sim 1/\sqrt{k_p\rho}$ (according to the radiation boundary condition). This scaling behavior results in the following expressions:

$$\frac{\partial e_{\rho,\phi,z}}{\partial\rho} \propto \frac{1}{(k_p\rho)^{3/2}} << e_{\rho,\phi,z}, \quad \frac{\partial h_{\rho,\phi,z}}{\partial\rho} \propto \frac{1}{(k_p\rho)^{3/2}} << h_{\rho,\phi,z}. \quad \text{(S5)}$$

Therefore, we can neglect the partial derivatives above, and the induction fields of the scattered SW in the far field (on the yellow ribbon in Supplementary Fig. 1, where $\rho\to\infty$) are calculated as

$$\mathbf{D}^{(s)} = \frac{i}{\omega}\nabla\times\mathbf{H}^{(s)} = \frac{i}{\omega}(-\partial_z h_\phi, \partial_z h_\rho - ik_p h_z, ik_p h_\phi)^T e^{ik_p\rho},$$
$$\mathbf{B}^{(s)} = -\frac{i}{\omega}\nabla\times\mathbf{E}^{(s)} = -\frac{i}{\omega}(-\partial_z e_\phi, \partial_z e_\rho - ik_p e_z, ik_p e_\phi)^T e^{ik_p\rho}. \quad \text{(S6)}$$

For the FPWs, in the spherical coordinate, the EM fields in the far field are expressed as

$$\mathbf{E}^{(f)}(\theta,\phi) = \mathbf{a}_n\frac{e^{ik_f R}}{R}, \quad \mathbf{H}^{(f)}(\theta,\phi) = \mathbf{b}_n\frac{e^{ik_f R}}{R}, \quad \text{(S7)}$$

where $\mathbf{a}_n, \mathbf{b}_n$ are complex vectors depend on the direction vector

$\hat{n} = \sin\theta\cos\phi\hat{x} + \sin\theta\sin\phi\hat{y} + \cos\theta\hat{z}$, k_f is the freely propagating wavenumber which equals k_0 in air and $\sqrt{\varepsilon}\sqrt{\mu}k_0$ inside the metamaterial, and the superscript (*f*) indicates that these quantities correspond to the FPWs. In the far field region, the radiation fields inside the isoptropic medium are transverse fields, satisfying

$$\hat{n}\cdot\mathbf{a}_n = \hat{n}\cdot\mathbf{b}_n = 0, \quad \mathbf{b}_n = \frac{1}{Z_f}\hat{n}\times\mathbf{a}_n, \tag{S8}$$

where $Z_f = Z_0 = \sqrt{\mu_0/\varepsilon_0}$ in air and $Z_f = \sqrt{\mu/\varepsilon}Z_0$ inside the metamaterial.

With the given expressions for the electromagnetic (EM) fields and induction fields, we can derive the expression for the longitudinal optical force. Since the total EM fields comprise three different types of fields, the Minkowski stress tensor can be divided into six components as follows:

$$\ddot{\mathbf{T}}^{\min} = \ddot{\mathbf{T}}^{(i)} + \ddot{\mathbf{T}}^{(s)} + \ddot{\mathbf{T}}^{(f)} + \ddot{\mathbf{T}}^{(is)} + \ddot{\mathbf{T}}^{(if)} + \ddot{\mathbf{T}}^{(sf)}, \tag{S9}$$

which are in terms of the pure incident SW $\ddot{\mathbf{T}}^{(i)}$, the pure scattered SW $\ddot{\mathbf{T}}^{(s)}$, the pure FPW $\ddot{\mathbf{T}}^{(f)}$, the interference of the incident SW and scattered SW $\ddot{\mathbf{T}}^{(is)}$, the interference of the incident SW and FPW $\ddot{\mathbf{T}}^{(if)}$, and interference of the scattered SW and FPW $\ddot{\mathbf{T}}^{(sf)}$, respectively. However, due to the conservation law of linear momentum in the absence of particle, the integral over $\ddot{\mathbf{T}}^{(i)}$ is zero.

A. Integral of $\ddot{\mathbf{T}}^{(s)}$

As the SW rapidly diminishes as $z \to \pm\infty$, $\ddot{\mathbf{T}}^{(s)}$ is nonzero only on the yellow ribbon as shown in Supplementary Fig. 1. As $R \to \infty$, this yellow ribbon becomes an infinitely long cylindrical surface extending along the *z* direction. Consequently, the integral of $\ddot{\mathbf{T}}^{(s)}$ can be expressed as

$$F_x^{(s)} = \lim_{R\to\infty}\int_{-\infty}^{\infty} dz \int_0^{2\pi} \hat{x}\cdot\ddot{\mathbf{T}}^{(s)}\cdot\hat{e}_\rho R d\phi = \lim_{R\to\infty}\int_{-\infty}^{\infty} dz \int_0^{2\pi} T_{x\rho}^{(s)} R d\phi. \tag{S10}$$

Using the expression of Minkowski stress tensor, one has

$$T_{x\rho}^{(s)} = \frac{1}{2}\mathrm{Re}[E_x^{(s)} D_\rho^{(s)*} + H_x^{(s)*} B_\rho^{(s)} - \frac{1}{2}(\mathbf{E}^{(s)}\cdot\mathbf{D}^{(s)*} + \mathbf{H}^{(s)*}\cdot\mathbf{B}^{(s)})\cos\phi]. \tag{S11}$$

Inserting Equations (S4) and (S6) into Equation (S11), one obtains

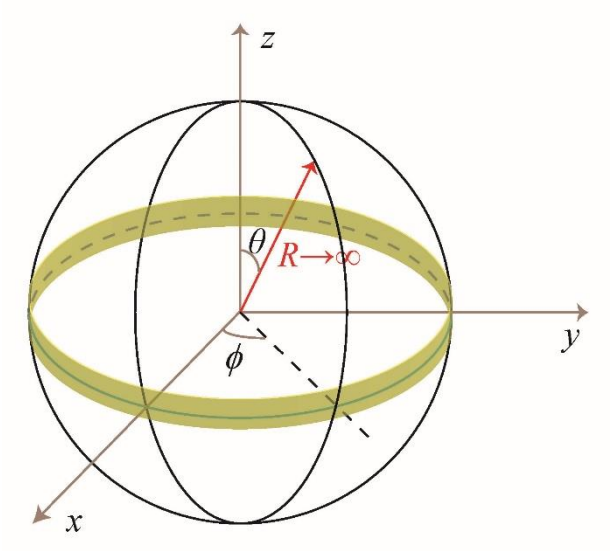

Supplementary Figure 1. The geometry of the integral surface. The yellow ribbon denotesa cylindrical surface with infinite radius and height. The SWs are vanishing except on the yellow ribbon. Therefore, the effective integral region of stress tensors involving the SWs is the yellow ribbon.

$$T_{x\rho}^{(s)} = \frac{1}{4\omega}\mathrm{Re}[2k_p \cos\phi(e_z h_\phi^* - e_\phi h_z^*) + i\cos\phi\partial_z(e_\rho h_\phi^* + e_\phi h_\rho^*) - 2i\sin\phi\partial_z(e_\phi h_\phi^*)]. \tag{S12}$$

Then,

$$\begin{aligned} F_x^{(s)} &= \lim_{R\to\infty} R\int_0^{2\pi} d\phi \frac{1}{4\omega}\mathrm{Re}[i\cos\phi(e_\rho h_\phi^* + e_\phi h_\rho^*) - 2i\sin\phi e_\phi h_\phi^*]\Big|_{z=-\infty}^{z=\infty} \\ &+ \frac{k_p}{\omega}\lim_{R\to\infty} R\int_{-\infty}^{\infty} dz\int_0^{2\pi} d\phi\cos\phi\frac{1}{2}\mathrm{Re}(e_z h_\phi^* - e_\phi h_z^*) \\ &= 0 - 0 + \frac{k_p}{\omega}\lim_{R\to\infty} R\int_{-\infty}^{\infty} dz\int_0^{2\pi} d\phi\cos\phi(-s_\rho^{(s)}) = -\frac{k_p}{\omega}\langle\cos\phi\rangle W_{sca}^{(s)}, \end{aligned} \tag{S13}$$

where we have used that the fields vanish at $z\to\pm\infty$, $s_\rho^{(s)} = -\frac{1}{2}\mathrm{Re}(e_z h_\phi^* - e_\phi h_z^*)$ is the radial component energy flux density induced by the scattered SW, $\langle\cos\phi\rangle$ is the averaged cosin of scattering angle, and

$$W_{sca}^{(s)} = \lim_{R\to\infty} R\int_{-\infty}^{\infty} dz\int_0^{2\pi} d\phi s_\rho^{(s)}, \tag{S14}$$

is the the rate at which photon energy is scattered in the form of SW. Since the system does not possess any gain, the scattered waves are radiated to infinity. As a result, the

radial energy flux density, denoted as $s_\rho^{(s)}$, is required to be positive. Similarly, the scattered power, represented by $W_{sca}^{(s)}$, must also be positive.

B. Integral of $\ddot{\mathbf{T}}^{(f)}$

For $\ddot{\mathbf{T}}^{(f)}$ in terms of the pure FPWs, since the FPWs do not decay away from the interface, the integral should be over the whole spherical surface S_∞. Using Equation (S7) and expression of Minkowski stress tensor, one has

$$\begin{aligned}\hat{x}\cdot\ddot{\mathbf{T}}^{(f)}\cdot\hat{n} &= \frac{1}{2}\mathrm{Re}[(\hat{x}\cdot\mathbf{E}^{(f)})(\mathbf{D}^{(f)*}\cdot\hat{n})+(\hat{x}\cdot\mathbf{H}^{(f)})(\mathbf{B}^{(f)*}\cdot\hat{n}) \\ &\quad -\frac{1}{2}(\mathbf{E}^{(f)}\cdot\mathbf{D}^{(f)*}+\mathbf{H}^{(f)}\cdot\mathbf{B}^{(f)*})(\hat{x}\cdot\hat{n})] \\ &= -\frac{1}{4}\mathrm{Re}(\mathbf{E}^{(f)}\cdot\mathbf{D}^{(f)*}+\mathbf{H}^{(f)}\cdot\mathbf{B}^{(f)*})\sin\theta\cos\phi,\end{aligned} \tag{S15}$$

where we have used Equation (S8). Note that

$$\begin{aligned}\mathbf{E}^{(f)}\cdot\mathbf{D}^{(f)*}+\mathbf{H}^{(f)}\cdot\mathbf{B}^{(f)*} &= \frac{1}{R^2}(\varepsilon_f\varepsilon_0|\mathbf{a}_{\hat{n}}|^2+\mu_f\mu_0|\mathbf{b}_{\hat{n}}|^2) \\ &= \frac{2}{R^2}\mu_f\mu_0|\mathbf{b}_{\hat{n}}|^2=\frac{2}{R^2}\frac{k_f}{\omega}Z_f|\mathbf{b}_{\hat{n}}|^2,\end{aligned} \tag{S16}$$

where $(\varepsilon_f,\mu_f)=(1,1)$ in air and $(\varepsilon_f,\mu_f)=(\varepsilon,\mu)$ inside the metamaterial, and the outward energy flux density of the PFW:

$$s_{\hat{n}}^{(f)}=\frac{1}{2}\mathrm{Re}(\mathbf{E}^{(f)}\times\mathbf{H}^{(f)*})=\frac{1}{2R^2}Z_f|\mathbf{b}_{\hat{n}}|^2>0, \tag{S17}$$

then the integral can be partitioned into two components: one over the upper half-space (air domain) and the other over the lower half-space (metamaterial domain):

$$\begin{aligned}F_x^{(f)} &= \oiint_{S_\infty}\hat{x}\cdot\ddot{\mathbf{T}}^{(f)}\cdot\hat{n}dS=-\frac{1}{c}\iint_{S_{upper}}s_{\hat{n}}^{(f)}\sin\theta\cos\phi dS-\frac{1}{v_f}\iint_{S_{lower}}s_{\hat{n}}^{(f)}\sin\theta\cos\phi dS \\ &= -\frac{1}{c}W_{sca}^{(f,a)}\langle\cos\vartheta\rangle_1-\frac{1}{v_f}W_{sca}^{(f,m)}\langle\cos\vartheta\rangle_2,\end{aligned} \tag{S18}$$

where $v_f=\omega/k_f$ is the phase speed of FPW inside the metamaterial, $W_{sca}^{(f,a)}, W_{sca}^{(f,m)}$ denote the rates at which photon energy is scattered to FPWs in air and the metamaterial, respectively, $\langle\cos\vartheta\rangle_1$ and $\langle\cos\vartheta\rangle_2$ correspond to the averaged cosines of the scattered angles, and $\vartheta=\cos^{-1}(\sin\theta\cos\phi)$ represents the scattered angle with respect to the x

axis. Since $s_{\hat{n}}^{(f)} > 0$ according to Equation (S17), the scattering rates $W_{sca}^{(f,a)}, W_{sca}^{(f,m)}$ are both positive.

C. Integral of $\ddot{\mathbf{T}}^{(is)}$

Since the SWs vanish at the infinities $z \to \pm\infty$, the effective integral of $\ddot{\mathbf{T}}^{(is)}$ is also performed on the yellow ribbon, which is an infinite cylindrical surface:

$$F_x^{(is)} = \lim_{R\to\infty} \int_{-\infty}^{\infty} dz \int_0^{2\pi} d\phi R\hat{x} \cdot \ddot{\mathbf{T}}^{(is)} \cdot \hat{e}_\rho = \lim_{R\to\infty} \int_{-\infty}^{\infty} dz \int_0^{2\pi} d\phi R(T_{xx}^{(is)} \cos\phi + T_{xy}^{(is)} \sin\phi). \tag{S19}$$

According to the expressions of the incident and scattered SWs, see Equations (S2)-(S6), $T_{xx}^{(is)}$ can be divided into two components as follows:

$$T_{xx}^{(is)} = \frac{1}{2}\mathrm{Re}[\, f_1(\phi) e^{ik_p R(1-\cos\phi)} + f_2(\phi) e^{-ik_p R(1-\cos\phi)}\,], \tag{S20}$$

where $f_1(\phi)$ and $f_2(\phi)$ are the total amplitudes of terms with phases $e^{\pm ik_p R(1-\cos\phi)}$, respectively. Using the method of stationary phase [1], we obtain

$$\begin{aligned}
&\lim_{R\to\infty} \int_0^{2\pi} d\phi R f_1(\phi) e^{ik_p R(1-\cos\phi)} \cos\phi \sim R\sqrt{\frac{2\pi}{k_p R}}\left[\, f_1(0) e^{i\pi/4} - f_1(\pi) e^{2ik_p R} e^{-i\pi/4}\,\right], \\
&\lim_{R\to\infty} \int_0^{2\pi} d\phi R f_2(\phi) e^{-ik_p R(1-\cos\phi)} \cos\phi \sim R\sqrt{\frac{2\pi}{k_p R}}\left[\, f_2(0) e^{i\pi/4} - f_2(\pi) e^{-2ik_p R} e^{-i\pi/4}\,\right].
\end{aligned} \tag{S21}$$

Therefore,

$$\begin{aligned}
&\lim_{R\to\infty} \int_0^{2\pi} d\phi R T_{xx}^{(is)} \cos\phi \\
&\sim R\sqrt{\frac{2\pi}{k_p R}} \frac{1}{2} \mathrm{Re}\left\{[\, f_1(0) + f_2(0)] e^{i\pi/4} - [\, f_1(\pi) e^{2ik_p R} + f_2(\pi) e^{-2ik_p R}\,] e^{-i\pi/4}\right\}.
\end{aligned} \tag{S22}$$

Similarly, we easily obtain that

$$\lim_{R\to\infty} \int_0^{2\pi} d\phi R T_{xy}^{(is)} \sin\phi \sim 0. \tag{S23}$$

Using Equations (S2)-(S6), we obtain

$$\begin{aligned}
f_1(0) + f_2(0) &= \frac{1}{2\omega}[2k_p(e_z h_{iy}^* - e_\phi h_{iz}^* + e_{iz} h_\phi^* - e_{iy} h_z^*) + i\partial_z(e_{ix} h_\phi^* + e_{iy} h_\rho^* + e_\phi h_{ix}^* + e_\rho h_{iy}^*)]\Big|_{\phi=0}, \\
f_1(\pi) e^{2ik_p R} + f_2(\pi) e^{-2ik_p R} &= \frac{-i}{2\omega}[\partial_z(e_{ix} h_\phi^* + e_{iy} h_\rho^*) e^{2ik_p R} + \partial_z(e_\phi h_{ix}^* + e_\rho h_{iy}^*) e^{-2ik_p R}]\Big|_{\phi=\pi}.
\end{aligned} \tag{S24}$$

Thus

$$
\begin{aligned}
F_x^{(is)} \sim & R\sqrt{\frac{2\pi}{k_p R}}\Big[\frac{k_p}{\omega}\frac{1}{2}\mathrm{Re}\int_{-\infty}^{\infty} dz(e_z h_{iy}^* - e_\phi h_{iz}^* + e_{iz} h_\phi^* - e_{iy} h_z^*)_{\phi=0} e^{i\pi/4} \\
& + \frac{1}{2}\mathrm{Re}[ie^{i\pi/4}(e_{ix} h_\phi^* + e_{iy} h_\rho^* + e_\phi h_{ix}^* + e_\rho h_{iy}^*)_{\phi=0}\Big|_{z=-\infty}^{z=\infty}] \\
& + \frac{1}{2}\mathrm{Re}[\frac{i}{4\omega}e^{-i\pi/4}[(e_{ix} h_\phi^* + e_{iy} h_\rho^*)e^{2ik_p R} + (e_\phi h_{ix}^* + e_\rho h_{iy}^*)e^{-2ik_p R}]_{\phi=\pi}\Big|_{z=-\infty}^{z=\infty} \\
\sim & \frac{k_p}{\omega} R\sqrt{\frac{2\pi}{k_p R}}\Big[\frac{1}{2}\mathrm{Re}\int_{-\infty}^{\infty} dz(e_z h_{iy}^* - e_\phi h_{iz}^* + e_{iz} h_\phi^* - e_{iy} h_z^*)_{\phi=0} e^{i\pi/4}.
\end{aligned}
\tag{S25}
$$

Here, leveraging the fact that the fields vanish as $z \to \pm\infty$, the second and third terms in the middle of Equation (S25) are zero. In the following, we will prove that the term with underline in Equation (S25) is just the extinction rate W_{ext} of the particle in the system.

The extinction rate W_{ext} is consist of two parts: $W_{ext}^{(is)}$ involving the incident and scattered SWs and $W_{ext}^{(if)}$ involving the incident SW and scattered FPWs. For $W_{ext}^{(is)}$, according to the definition [2],

$$
W_{ext}^{(is)} = -\int_{-\infty}^{\infty} dz \int_0^{2\pi} R d\phi s_\rho^{(is)}, \tag{S26}
$$

where $s_\rho^{(is)} = \frac{1}{2}\mathrm{Re}(\mathbf{E}^{(i)} \times \mathbf{H}^{(s)*} + \mathbf{E}^{(s)} \times \mathbf{H}^{(i)*}) \cdot \hat{\rho} = \mathbf{s}^{(is)} \cdot \hat{\rho}$ is the outward (radial) energy flux density by the mixing of incident and scattered SWs. Similary, $s_\rho^{(is)}$ can also be devided into two components according to their phases as

$$
s_\rho^{(is)} = \frac{1}{2}\mathrm{Re}[\tilde{f}_1(\phi)e^{ik_p R(1-\cos\phi)} + \tilde{f}_2(\phi)e^{-ik_p R(1-\cos\phi)}], \tag{S27}
$$

where according to Equations (S2)-(S6),

$$
\tilde{f}_1(\phi) = e_\phi h_{iz}^* - e_z(h_{iy}^* \cos\phi - h_{ix}^* \sin\phi), \quad \tilde{f}_2(\phi) = (e_{iy} \cos\phi - e_{ix} \sin\phi)h_z^* - e_{iz} h_\phi^*. \tag{S28}
$$

Using the method of stationary phase [1], $W_{ext}^{(is)}$ is calculated as

$$
W_{ext}^{(is)} \sim -R\sqrt{\frac{2\pi}{k_p R}}\frac{1}{2}\mathrm{Re}\int_{-\infty}^{\infty} dz\Big\{[\tilde{f}_1(0) + \tilde{f}_2(0)]e^{i\pi/4} + [\tilde{f}_1(\pi)e^{2ik_p R} + \tilde{f}_2(\pi)e^{-2ik_p R}]e^{-i\pi/4}\Big\}. \tag{S29}
$$

Since the extinction rate is independent of *R*, the last two terms in Equation (S29),

which oscillate with R, make no contribution to $W_{ext}^{(is)}$. Therefore, substituting Equation (S28) into Equation (S29), we obtain

$$W_{ext}^{(is)} \sim R\sqrt{\frac{2\pi}{k_p R}}\frac{1}{2}\mathrm{Re}\int_{-\infty}^{\infty} dz(e_z h_{iy}^* - e_\phi h_{iz}^* + e_{iz} h_\phi^* - e_{iy} h_z^*)_{\phi=0} e^{i\pi/4}, \tag{S30}$$

which is just the underlined term in Equation (S25). On the other hand, since $|k_p| > |k_f|$, based on the method of stationary phase, it is easy to know that the extinction rate $W_{ext}^{(if)} = 0$. Therefore,

$$F_x^{(is)} = \frac{1}{v_p}(W_{ext}^{(is)} + W_{ext}^{(if)}) = \frac{1}{v_p}W_{ext} = -\frac{1}{v_p}\int_{-\infty}^{\infty} dz \int_0^{2\pi} Rs_\rho^{(is)} d\phi. \tag{S31}$$

D. Integrals of $\ddot{\mathbf{T}}^{(if)}$ and $\ddot{\mathbf{T}}^{(sf)}$

The effective integrals of $\ddot{\mathbf{T}}^{(if)}$ and $\ddot{\mathbf{T}}^{(sf)}$ are also on the yellow ribbon. We can infer that these two integrals are both zero based upon a simple argument. Note that in the far field region $R \to \infty$,

$$\mathbf{A}^{(s)} \sim \sqrt{\frac{1}{k_p R}}, \quad \mathbf{A}^{(f)} \sim \frac{1}{k_f R}, \tag{S32}$$

where $\mathbf{A} = \mathbf{E}, \mathbf{H}, \mathbf{D}, \mathbf{B}$. Therefore, the FPWs are infinitesimal compared with the SWs on the effective integral surface. Then, $\ddot{\mathbf{T}}^{(if)}, \ddot{\mathbf{T}}^{(sf)}$ are also infinitesimal compared with $\ddot{\mathbf{T}}^{(is)}$, leading to

$$F_x^{(if)} \sim \sqrt{\frac{1}{k_f R}}F_x^{(is)} \sim 0, \qquad F_x^{(sf)} \sim \sqrt{\frac{1}{k_f R}}F_x^{(is)} \sim 0. \tag{S33}$$

E. The total force

To sum up, the longitudinal optical force is given by

$$\begin{aligned} F_x &= F_x^{(is)} + F_x^{(s)} + F_x^{(f)} \\ &= \underbrace{\frac{1}{v_p}W_{ext}}_{\text{incdident force}} - \underbrace{\left(\frac{1}{v_p}W_{sca}^{(s)}\langle\cos\phi\rangle + \frac{1}{c}W_{sca}^{(f,a)}\langle\cos\vartheta\rangle_1 + \frac{1}{v_f}W_{sca}^{(f,m)}\langle\cos\vartheta\rangle_2\right)}_{\text{recoil force}}. \end{aligned} \tag{S34}$$

Similar to the optical force in air, the first part of F_x, i.e $F_x^{(is)}$, which is caused by the

incident photons, is the incident optical force, and the second and third parts, i.e $F_x^{(s)}, F_x^{(f)}$, which are due to the scattered photons, contribute to the recoil optical force. A more comprehensive and detailed discussion will be provided in the subsequent section.

Supplementary Note 2： The conservation of canonical momentum

In this section, we will establish the relationship between the longitudinal optical force and the canonical momentum of light. In general, the constitutive relations for an anisotropic medium can be expressed as follows:

$$\begin{pmatrix} \mathbf{D} \\ \mathbf{B} \end{pmatrix} = \begin{pmatrix} \ddot{\varepsilon}\varepsilon_0 & 0 \\ 0 & \ddot{\mu}\mu_0 \end{pmatrix} \begin{pmatrix} \mathbf{E} \\ \mathbf{H} \end{pmatrix}, \tag{S35}$$

where $\ddot{\varepsilon}, \ddot{\mu}$ are relative permittivity and permeability tensors. The energy density W and canonical mometum density $\mathbf{g}^{\min}$ in the medium are given by

$$W = \mathrm{Re}\langle \psi \,|\, \omega\psi \rangle, \quad \mathbf{g}^{\min} = \mathrm{Re}\langle \psi \,|\, \hat{p}\psi \rangle, \tag{S36}$$

where $\hat{p} = -i\nabla$ is the canonical momentum operator, and

$$|\psi\rangle = \begin{pmatrix} \sqrt{\tilde{\varepsilon}\varepsilon_0} & 0 \\ 0 & \sqrt{\tilde{\mu}\mu_0} \end{pmatrix} \begin{pmatrix} \mathbf{E} \\ \mathbf{H} \end{pmatrix}, \tag{S37}$$

with

$$\tilde{\varepsilon} = \frac{\partial}{\partial\omega}(\omega\ddot{\varepsilon}), \quad \tilde{\mu}\frac{\partial}{\partial\omega}(\omega\ddot{\mu}). \tag{S38}$$

Therefore, for a wave with a space-dependence $e^{i\mathbf{k}\cdot\mathbf{r}}$ (wave vector is $\mathbf{k}$), the relation between the energy density and canonical momentum density is [3]

$$\mathbf{g}^{\min} = \frac{\mathbf{k}}{\omega} W. \tag{S39}$$

On the other hand, the group speed of an EM wave along the propagating direction is defined as

$$v_g = \frac{s_{\hat{n}}}{W}, \tag{S40}$$

where $s_{\hat{n}}$ is the energy flux density along the propagating direction. As such,

$$\frac{\mathbf{k}}{\omega} s_{\hat{n}} = v_g \mathbf{g}^{\min}, \tag{S41}$$

which denotes the canonical momentum flux density along the propagating direction.

Inserting Equation (S41) into Equation (S31), we obtain

$$F_x^{(is)} = -\frac{k_p}{\omega} \lim_{R\to\infty} \int_{-\infty}^{\infty} dz \int_0^{2\pi} R s_\rho^{(is)} d\phi = -\lim_{R\to\infty} \int_{-\infty}^{\infty} dz \int_0^{2\pi} R v_g^{(s)} g_x^{(is)} d\phi, \tag{S42}$$

where $v_g^{(s)}$ is the group speed of the SW, $g_x^{(is)}$ is the canonical momentum density associate with the mixing fields, which is contributed from the incident SW. The negative sign in Equation (S42) indicates that the canonical momentum is injected into the space. Therefore, $F_x^{(is)}$ corresponds to the canonical momentum transfer resulting from directly capturing the incident photons, and it can be called the inicident force. Inserting Equation (S41) into Equations (S13) and (S18), we obtain

$$\begin{aligned} F_x^{(s)} &= -\lim_{R\to\infty} \int_{-\infty}^{\infty} dz \int_0^{2\pi} R v_g^{(s)} g^{(s)} \cos\phi d\phi = -\lim_{R\to\infty} \int_{-\infty}^{\infty} dz \int_0^{2\pi} R v_g^{(s)} g_x^{(s)} d\phi, \\ F_x^{(s)} &= -\oiint_{S_\infty} v_g^{(f)} g_{\hat{n}}^{(f)} \cos\vartheta dS = -\oiint_{S_\infty} v_g^{(f)} g_{\hat{n}x}^{(f)} dS, \end{aligned} \tag{S43}$$

where $g^{(s)}, g_{\hat{n}}^{(f)}$ are the canonical momentum densities of the scattered SW and FPW along their propagating directions, and $g_x^{(s)}, g_{\hat{n}x}^{(f)}$ are the corresponding projections along the *x* direction. Thus, $F_x^{(s)}$ and $F_x^{(f)}$ corresponds to the canonical momentum transfer due to reemitting the captured photons, and they are recoil force.

Equations (S42) and (S43) establishes a relationship between the longitudinal optical force and the change in the canonical momentum of light throughout space, encompassing both the SWs and the bulk waves (FPWs), per unit time. Hence, it can be concluded that the longitudinal optical force is entirely attributable to the canonical momentum of light.

Supplementary Note 3： Trajectory of the particle near the substrate

For the dielectric constant of the particle, namely $\varepsilon_r = 3$ and $\varepsilon_r = 15$, the lack of equilibrium along the *y* direction, as indicated by the black and blue lines in Fig. 3**c** of the main text, causes the particles to ultimately come into contact with the surface of the metamaterial, as shown in Supplementary Figs. 2**a** and 2**c**. In contrast, for $\varepsilon_r = 9$, the particle oscillates around the equilibrium position along the *y* direction. Due to the negligible ambient damping force compared to the optical force, the particle can rapidly move far along the negative-*x* direction within a short time period. However, when we reduce the amplitude of the light source by two orders (resulting in a four-order reduction in the optical force), the ambient damping force becomes significant. As depicted by the purple dashed line in Supplementary Fig. 2**b**, under the reduced light source, the particle moves much slower along the *x* direction, and eventually becomes confined to approximately $y \sim 1.12\mu m$.

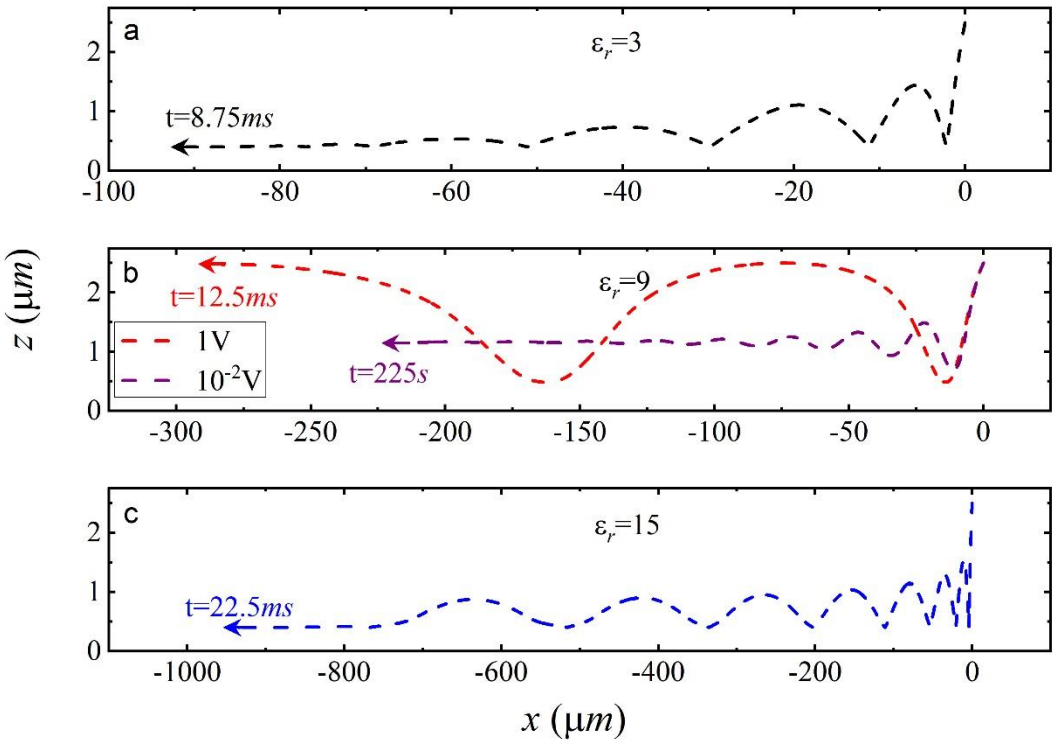

Supplementary Figure 2. The trajectories of the particles with different relative permittivities. a $\varepsilon_r = 3$, **b** $\varepsilon_r = 9$ and **c** $\varepsilon_r = 15$. The radius and mass density of the

particles are $r = 0.7\mu m$ and $\rho = 2500\text{kg}/m^3$, and they are initially located at $(x_0, y_0) = (0, 2.5)\mu m$ with zero velocity. The ambient damping constant is used as $\gamma = 20pN/\mu m^2$. The amplitudes of the line sources for the black, red and blue curves are 1V, and 0.01V for the purple curve. The coefficient of restitution we used is $e = 0.7$. The arrows denote the directions of movements. The consumed time form the starting point to the ends of the trajectories are indicated. (Source data are provided as a Source Data file).

Supplementary Note 4： Metamaterial based on a composite metamaterial host

In the realm of high frequency, locating an exceptionally high dielectric medium is nearly unattainable. Nevertheless, this host medium boasting a substantial relative permittivity can be substituted with a composite metamaterial.

The unit cell of the metamaterial supporting the TM-polarized OSTB is depicted in Supplementary Fig. 3a. The white circle represents the air hole, while the gray region containing embedded black disks serves as the host medium. In this context, the gray region represents dielectric inclusions, while the black disks signify metallic inclusions. The effective permittivity of the composite host medium is determined by the Maxwell-Garnett formula, which is expressed as follows:

$$\varepsilon_b = \varepsilon_d \frac{2p(\varepsilon_m - \varepsilon_d) + \varepsilon_m + 2\varepsilon_d}{2\varepsilon_d + \varepsilon_m - p(\varepsilon_m - \varepsilon_d)}, \tag{S44}$$

where p represents the filling ratio of the metallic inclusions, ε_d is the relative permittivity of the dielectric, and ε_m is the relative permittivity of the metallic inclusions. In the lossless limit, the relative permittivity ε_m based on the Drude model is given by:

$$\varepsilon_m(\omega) = 1 - \frac{\omega_p^2}{\omega^2}, \tag{S45}$$

where ω_p is the plasmon resonance frequency. According to Eqs. (S44) and S(45), the host composite medium is dispersive. We use the coherent potential approximation method to calculate the effective constitutive parameters. According to Ref. [4], the effective constitutive parameters are obtained by

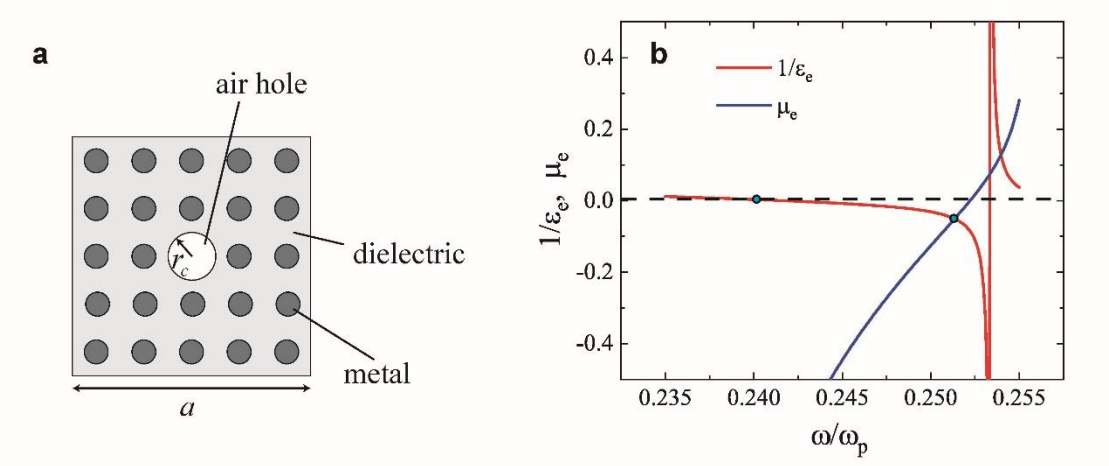

Supplementary Figure 3. Metamaterial design in high frequency regime. **a** The supercell of the metamaterial. **b** The effective constitutive parameters as functions of the frequency. The relative permittivity of the dielectric is $\varepsilon_d = 5$, the filling ratio of the metallic inclusions is $p = 0.2$, $a = 3c/\omega_p$, $r_c = 0.1a$. (Source data are provided as a Source Data file).

$$\begin{aligned}
&\frac{\frac{\varepsilon_e}{\varepsilon_b}+2\frac{J'_0(k_o r_o)}{k_o r_o J_0(k_o r_o)}}{\frac{\varepsilon_e}{\varepsilon_b}+2\frac{Y'_0(k_o r_o)}{k_o r_o Y_0(k_o r_o)}}=\frac{Y_0(k_o r_o)}{iJ_0(k_o r_o)}\frac{D_0}{1+D_0},\\
&\frac{\mu_e-\frac{J_1(k_o r_o)}{k_o r_o J'_1(k_o r_o)}}{\mu_e-\frac{Y_1(k_o r_o)}{k_o r_o Y'_1(k_o r_o)}}=\frac{Y_1(k_o r_o)}{iJ'_1(k_o r_o)}\frac{D_1}{1+D_1},
\end{aligned} \tag{S46}$$

where $r_o = a\sqrt{\pi}$, $k_o = \sqrt{\varepsilon_b}k_0$ is the wavenumber in the composite host medium, J_n, Y_n are the first and second kinds of Bessel functions, and D_n is the Mie coefficient of the air hollow in the backgroud medium given by

$$D_n = -\frac{m'J'_n(m'x)J_n(x)-J_n(m'x)J'_n(x)}{m'J'_n(m'x)H_n(x)-J_n(m'x)H'_n(x)}, \tag{S47}$$

where $m' = 1/\sqrt{\varepsilon_b}$, $x = k_o r_c$, and $H_n = J_n + iY_n$ is the first kind of Hankel function.

For given values of $\varepsilon_d = 5$, $p = 0.2$, $a = 3c/\omega_p$, and $r_c = 0.1a$, we calculate the effective constitutive parameters of the metamaterial using Eqs. (S44)-(S47) and present the results in Supplementary Fig. 3**b**. It can be observed that within a specific frequency range (between the two cyan dots), namely $0.240 \le \omega/\omega_p \le 0.251$, the conditions $-1 < \mu_e < \varepsilon_e^{-1} < 0$ are satisfied. This indicates that the TM polarized OSTB can be excited within this frequency range. Note that the valid frequency range can be adjusted by tuning the lattice constant *a*.

Supplementary Note 5: Prism excitation of OSTB on the surface of a metamaterial consist of a PC microstructure

Supplementary Fig. **4** shows the real parts of the electric fields in a region that is far away from the source region. It is observed that the FPWs are vanishingly small, and the electromagnetic (EM) field is dominated by the SW mode in this region.

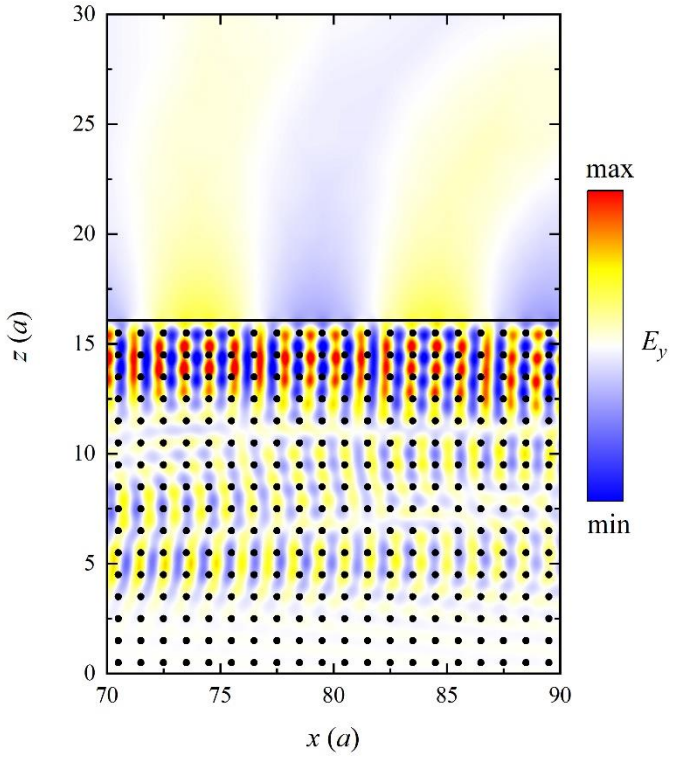

Supplementary Figure 4. An enlargement of a portion of Fig. 5a. The black disks are air holes and the horizontal black solid line represents the interface between the metamaterial and air. (Source data are provided as a Source Data file).

In Supplementary Fig. 5, we illustrate TM-polarized OSTBs excited using prisms. The wavenumber along the x direction inside the prism equals to that of the OSTB when the incident angle is 45°. At this incident angle, and with perfect TM polarization, excitation efficiency peaks. Deviation from this angle results in reduced excitation efficiency due to the wavenumber mismatch, as evident from the comparison between the Fourier spectra shown by the black lines in Supplementary Figs. 5**b** and 5d. Moreover, if the incident beam is not fully TM-polarized, scattering efficiency also diminishes, as depicted by the red line in Supplementary Fig. 5**b**.

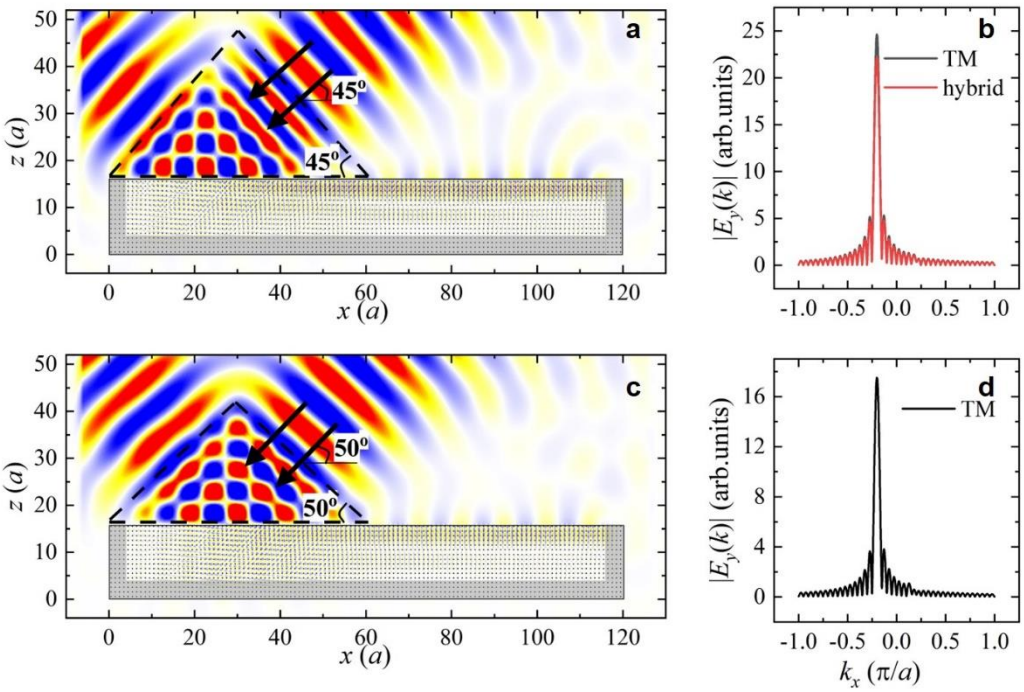

Supplementary Figure 5. TM-polarized OSTBs excited using prisms. **a** and **c,** The y-component electric field distributions. The black dashed line outlines the prism boundary, while white arrows indicate the directions of incident Gaussian beams. Both prisms have a refractive index of 1.69. The shaded regions are corresponding to the absorbing metamaterials. **b** and **d,** The Fourier transform spectra of the electric fields on the metamaterial surface ($70a \le x \le 110a, z = 16a$). In panel **b,** the black and red solid lines correspond to perfect TM-polarized and hybrid (81% TM + 19% TE) polarized incident beams, respectively. All incident beams have the same amplitude. (Source data are provided as a Source Data file).

Supplementary Note 6: Various types of particles pulled over the metamaterial with a microstructure

The longitudinal optical forces acting on individual particles with varying shapes and constitutive parameters are examined. Results for circular, square, and triangular particles are presented in Supplementary Figs. 6a, 6b, and 6c, respectively, with their

geometric parameters illustrated in the insets. We consider particles with transparent, lossy, and chiral (chirality parameter χ, expressed in units of 1/c) properties. For transparent and chiral particles which are assumed loessless, their refractive indices are required to be greater than 1 according to the causality. It is noted from Supplementary Fig. 6 that the longitudinal optical forces on single particles, irrespective of shape or constitutive parameters, are consistently negative.

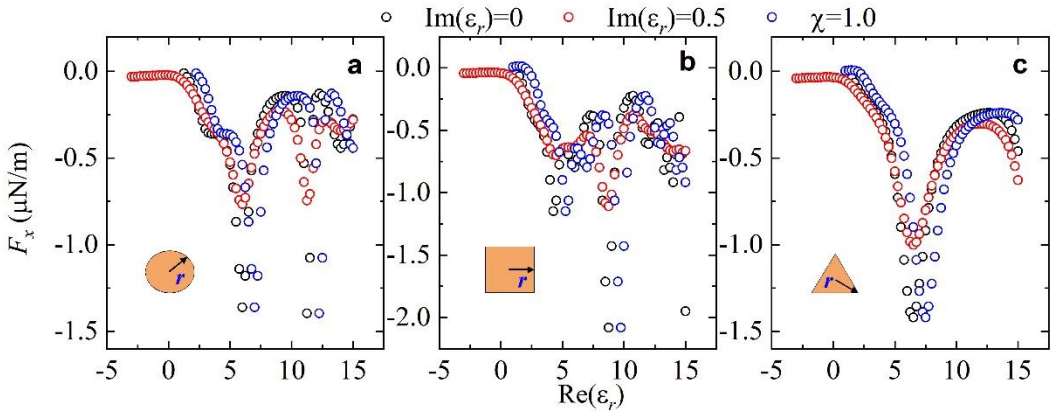

Supplementary Figure 6. **Optical pulling of particles with varied shapes**. The longitudinal optical forces on **a** circular, **b** square, and **c** triangular particles are plotted against their relative permittivity for a fixed particle size $k_0 r = 1.5$. Transparent, lossy, and chiral particles are represented by black, red, and blue circles, respectively. (Source data are provided as a Source Data file).

Additionally, we explore scenarios where multiple particles are arranged equidistantly along the *x*-direction, as depicted in the geometrical sketch in the inset of Supplementary Fig. 7**c**. The first particle is circular and transparent, the second particle is square and either lossy dielectric ($\mathrm{Re}(\varepsilon_r) > 0$) or plasmonic ($\mathrm{Re}(\varepsilon_r) < 0$), and the third particle is triangular and chiral. Notably, when the second particle is a lossy dielectric (panels **a**-**c** in Supplementary Fig. 7), the longitudinal optical forces on all particles remain negative, regardless of the distances (*d*) between them. However, when the

second particle is plasmonic (panel **d**), its longitudinal optical force can become positive for some distances (*d*). Nonetheless, the overall longitudinal optical force acting on the three particles remains negative.

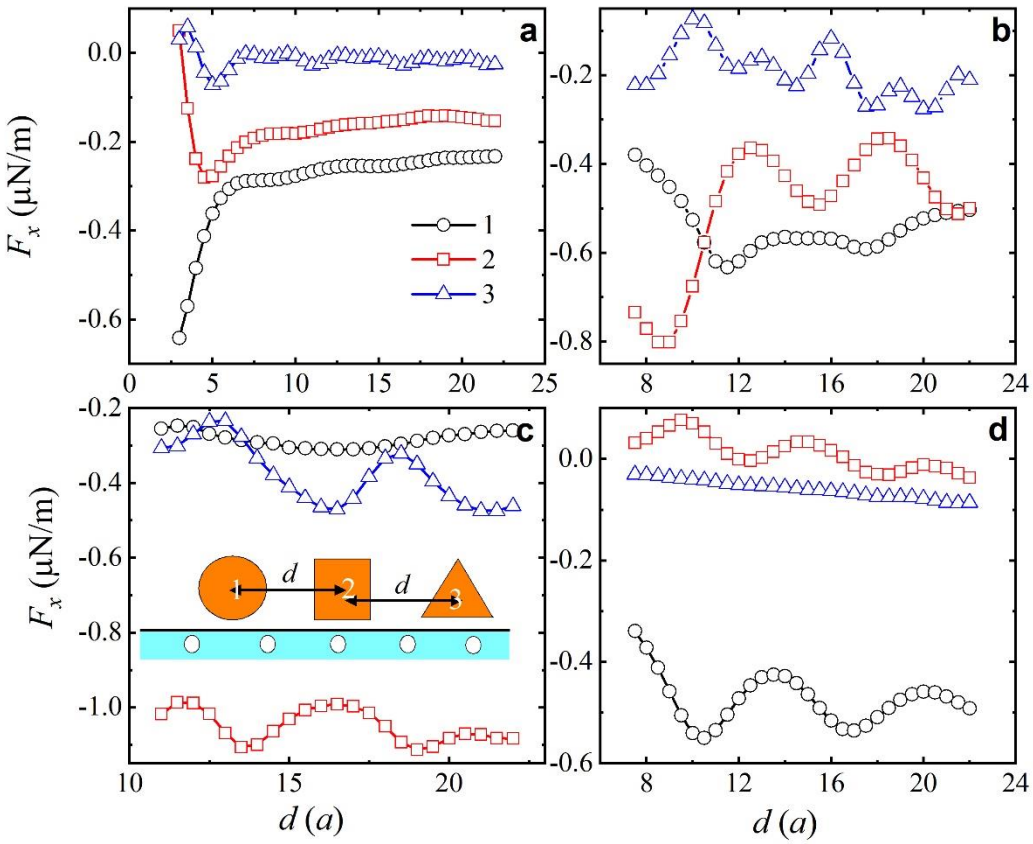

Supplementary Figure 7. **Optical pulling of multiple particles.** The longitudinal optical forces on three particles with particle sizes **a** $k_0 r = 0.5$, **b** and **d** $k_0 r = 1.5$, **c** $k_0 r = 2.5$. The inset in panel **c** illustrates the arrangement of the particles, equidistant along the *x*-direction. The first and third particles are transparent ($\varepsilon_r = 5, \chi = 0$) and chiral ($\varepsilon_r = 5, \chi = 1.0$), respectively. In panels (**a-c**), the relative permittivity of the middle particle is $\varepsilon_r = 5 + 0.5i$, while in panel **d** it is $\varepsilon_r = -3 + 0.5i$. (Source data are provided as a Source Data file).

Supplementary Note 7：　The effect of loss from the metamaterial

Now let's consider the case where the metamaterial exhibits loss. For a typical scenario, we assume the constitutive parameters of the metamaterial to be $\varepsilon = -0.9 + 0.02i$ and $\varepsilon = -1.2 + 0.02i$. Although the OSTB is still supported, its amplitude rapidly decreases as it propagates along the x direction, as illustrated in Supplementary Fig. 8**a**. The reduction in field amplitude results in a weakening of the optical force strength. However, it is important to note that the optical pulling effect remains valid for any passive particles. As depicted in Supplementary Figs. 8**b** and 8**c**, the longitudinal optical force is negative regardless of the dielectric constant, radius, and x coordinate of the particle, albeit the strength of the optical pulling force significantly diminishes when the particle is located further away from the light source.

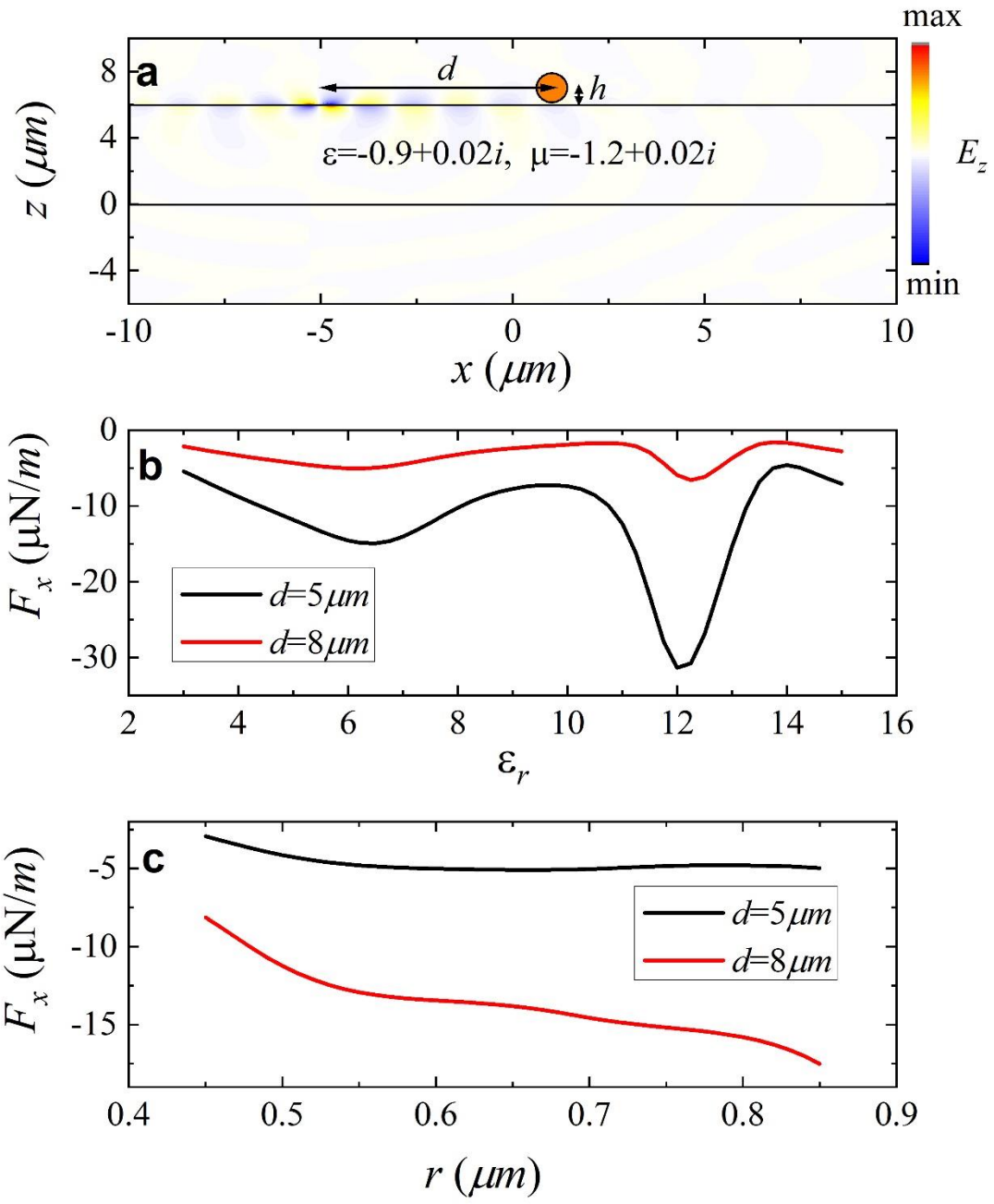

Supplementary Figure 8. In case of lossy metamaterial. The metamaterial is lossy with $\varepsilon = -0.9 + 0.02i$, $\varepsilon = -1.2 + 0.02i$. **a** The electric field. The longitudinal optical force as functions of (**b**) the relative permittivity of the particle and (**c**) the radius of the particle at different locations. (Source data are provided as a Source Data file).

Supplementary References:

[1] Born, M. & Wolf, E. Principles of optics: electromagnetic theory of propagation,

interference and diffraction of light (Elsevier, 2013).

[2] Bohren, C. F. & Huffman, D. R. Absorption and scattering of light by small particles (John Wiley & Sons, 2008).

[3] Bliokh, K. Y., Bekshaev, A. Y. & Nori, F. Optical momentum, spin, and angular momentum in dispersive media, Physical review letters 119, 073901 (2017).

[4] Wu, Y., Li, J., Zhang, Z.-Q. & Chan, C. T. Effective medium theory for magnetodielectric composites: Beyond the long-wavelength limit, Physical Review B 74, 085111 (2006).